Biocompatible Magnetofluorescent Probes: Luminescent Silicon Quantum Dots Coupled with Superparamagnetic Iron(III) Oxide

Folarin Erogbogbo,[†,§] Ken-Tye Yong,[§] Rui Hu,[§] Wing-Cheung Law,[§] Hong Ding,[§] Ching-Wen Chang,[†] Paras N. Prasad,[‡,§,*] and Mark T. Swihart[†,§,*]

[†]Department of Chemical and Biological Engineering, [‡]Department of Chemistry, and [§]Institute for Lasers, Photonics and Biophotonics, The University at Buffalo, State University of New York, Buffalo, New York 14260-4200

ABSTRACT Luminescent silicon quantum dots (SiQDs) are gaining momentum in bioimaging applications, based on their unique combination of optical properties and biocompatibility. Here, we report the development of a multimodal probe that combines the optical properties of silicon quantum dots with the superparamagnetic properties of iron oxide nanoparticles to create biocompatible magnetofluorescent nanoprobes. Multiple nanoparticles of each type are coencapsulated within the hydrophobic core of biocompatible phospholipid—polyethyleneglycol (DSPE-PEG) micelles. The size distribution and composition of the magnetofluorescent nanoprobes were characterized by transmission electron microscopy (TEM) and energy-dispersive X-ray spectroscopy (EDS). Enhanced cellular uptake of these probes in the presence of a magnetic field was demonstrated *in vitro*. Their luminescence stability in a prostate cancer tumor model microenvironment was demonstrated *in vivo*. This paves the way for multimodal silicon quantum-dot-based nanoplatforms for a variety of imaging and delivery applications.

KEYWORDS: silicon · quantum dots · superparamagnetic · iron oxide · nanoparticle · hybrid · multimodal

Quantum dots (QDs) are semiconductor nanomaterials that typically consist of combinations of elements from groups II and VI (CdSe, CdTe, CdS, ZnS, and ZnSe), groups IV and VI (PbS and PbSe), or groups III and V (GaAs, GaN, InP, and InAs) of the periodic table.[1,2] Their optical properties, including bright emission, photostability, size-dependent luminescence, and long fluorescence lifetimes, make them suitable for many bioimaging applications. Two topics of tremendous current interest are the improvement of their toxicity profile[3−6] and their use in multimodal nanoprobes that combine imaging and delivery or multiple imaging modalities in the same construct.[7] In particular, probes combining the superparamagnetism of iron oxide (Fe_3O_4 or Fe_2O_3) nanoparticles and optical properties of QDs have provided a single nanoscale platform with multimodal properties.[7−11] Fabrication of these probes is desirable for magnetic resonance contrast enhancement coupled with optical imaging,[7] biological separations,[10] magnetic manipulation of optical properties,[12] and capture of biologically relevant molecules.[13] The ease of manufacture and biocompatibility of Fe_3O_4 has led to its adoption for clinical use;[14] however, the toxicity concern associated with quantum dots is a remaining challenge, which limits the adoption of multimodal probes containing QDs.

A very promising direction is the use of heavy-metal-free semiconductor materials like nanoscale silicon.[15−17] Challenges associated with the synthesis of SiQDs with optical properties equivalent to those of Cd-based QDs are being overcome, increasingly enabling their application in biological systems.[17−19] In addition to the expected low toxicity of SiQDs, abundance of silicon and the inexpensive commodity chemicals required for its synthesis make it attractive.[20] Silicon is expected to be nontoxic compared to heavy-metal-based quantum dots[16,21] because bulk and porous silicon are nontoxic. *In vivo*, silicon ultimately degrades to silicic acid that is excreted through the urine.[17] SiQDs have been reported to be 10 times safer than Cd-based quantum dots *in vitro*.[16] An important step toward developing silicon quantum dots as a multifunctional probe was achieved by doping them with paramagnetic manganese.[22] An alternative means of achieving this is to coencapsulate SiQDs with magnetic nanoparticles, rather than doping a magnetic ion into the SiQDs themselves. This approach may provide higher

*Address correspondence to pnprasad@buffalo.edu, swihart@buffalo.edu.

Received for review May 10, 2010 and accepted August 18, 2010.

Published online August 25, 2010. 10.1021/nn101016f

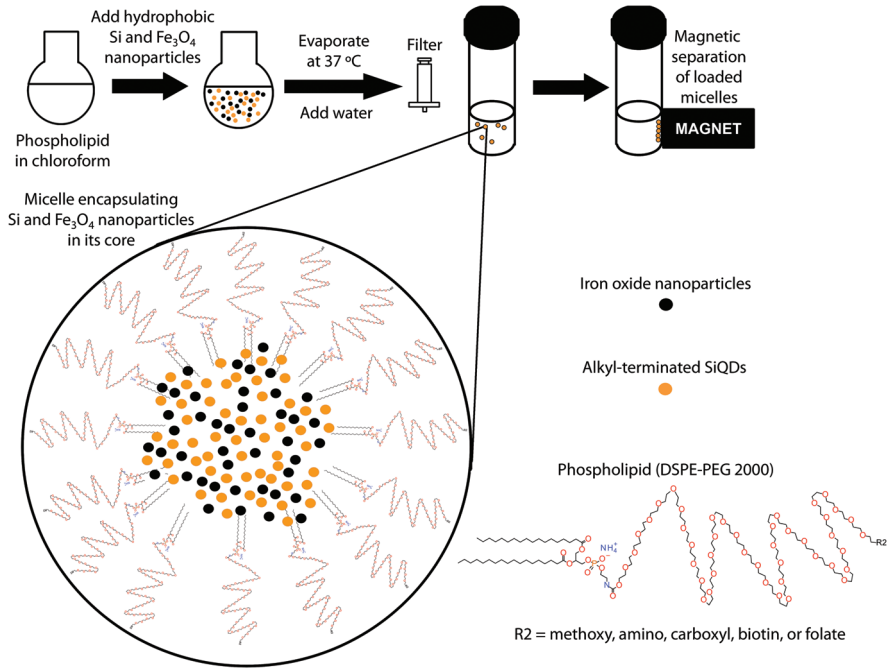

Scheme 1. Schematic diagrams illustrating preparation and the internal structure of micelle-coencapsulated silicon quantum dots and iron oxide. The strong interactions between the hydrophobic surface ligands on the nanoparticles and the alkyl chains of the phospholipid internalize the particles in the core of the micelle. Note that the phospholipid molecules and nanoparticles are not drawn to scale (in reality the relative size of the molecules is much smaller).

magnetization with less effect on the luminescence, compared to doping the quantum dots with magnetic ions.

We have previously demonstrated that phospholipid micelles are effective carriers of multiple silicon quantum dots.[15,20] The physicochemical properties of micelles formed from PEG-terminated phospholipids allow for excellent penetration, diffusion, stability, and circulation properties in biological environments because the biologically inert hydrophilic PEG groups are in contact with the environment. The low critical micelle concentration (CMC) for these PEGylated phospholipids reflects the fact that they form very stable and robust micelles, even at high dilution. Their surface can be functionalized with proteins, antibodies, aptamers, or peptides[15] to provide specific targeting. These micelles can transport hydrophobic materials entrapped within their hydrophobic core. This introduces the possibility of coencapsulating materials like magnetite or hydrophobic drugs like paclitaxel along with SiQDs.

Here we demonstrate preparation of SiQD-based hybrid nanoprobes combining luminescence with superparamagnetism, along with their use in proof-of-concept biological applications. With a unique synthesis method for SiQDs, we have overcome the challenges associated with achieving stable emission spanning the visible to the near-infrared (NIR) spectrum, maintaining dispersibility and stability in aqueous environments and combining SiQD optical properties with superparamagnetism. This work combines two of the most biocompatible quantum dots to create a multimodal probe that overcomes the concern of heavy metal toxicity. Its optical and magnetic properties were evaluated, and imaging was demonstrated in macrophage cells and live mice.

The interaction of hydrophobic SiQDs with amphiphilic phospholipid PEG produces micelles with multiple (>25) silicon quantum dots in the core. We refer to these as micelle-encapsulated silicon quantum dots (MSiQD).[15] This is not typical of previous reports of micelle-encapsulated quantum dots, where 1−4 dots were encapsulated in a micelle.[23] The interactions of the long hydrophobic chains on the silicon surface and the hydrophobic groups of the phospholipids are responsible for the localization of multiple SiQDs in the core of the micelle. This enables simultaneous coencapsulation of multiple copies of other hydrophobic entities within the core of the micelle. As illustrated in Scheme 1, hydrophobic-ligand-terminated silicon particles, mixed with hydrophobic-ligand-terminated iron oxide NPs, were sonicated with phospholipid PEG in chloroform. After evaporation and subsequent resuspension in water, both types of nanoparticles were entrapped in the hydrophobic core of the micelle to form micelle-coencapsulated silicon quantum dots and iron oxide nanoparticles (MSiQD-Mag).

RESULTS AND DISCUSSION

Characterization of Particles. Parts A and B of Figure 1 show transmission electron microscope images of the free-standing hydrophobic silicon quantum dots (terminated with ethyl undecylenate). The size of the silicon

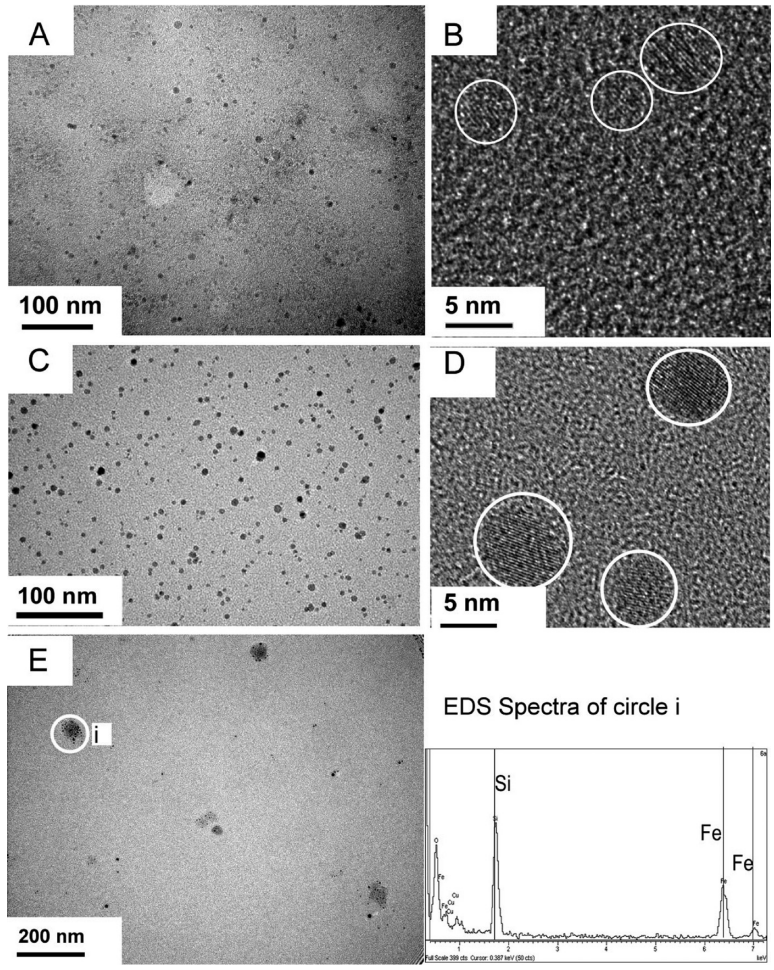

Figure 1. Characterization of nanoparticles and nanoprobes. Transmission electron microscope images in A and B show ethylundecylenate-grafted silicon quantum dots at different magnifications: (A) individual quantum dots separated from one another; (B) magnified view of A which displays the lattice fringes of the quantum dots. (C,D) Iron oxide nanoparticles at different magnification: (C) individual iron oxide nanoparticles; (D) higher magnification image showing lattice fringes of the iron oxide. (E) Micelle-coencapsulated silicon and iron oxide nanoparticles. (F) EDX analysis confirms the presence of silicon and iron in the micelle.

nanoparticles is ~4 nm, and the presence of lattice fringes demonstrates that they are crystalline. Figure 1C,D presents the iron oxide nanoparticles cast from chloroform. The particles are around 7 ± 2 nm in size. Figure 1E shows MSiQD-Mag. The micelles range in size from 50 to 100 nm when the two different nanomaterials are coencapsulated in the core. This size range is consistent with the size range of micelle-encapsulated silicon quantum dots without iron oxide nanoparticles, which may displace some of the silicon in the micelle. The hydrodynamic diameter distribution measured by dynamic light scattering (DLS) number measurements showed a mean diameter of 55 nm (Figure S1, Supporting Information). Even though the micelle size is relatively uniform, the ratio of Si to Fe_3O_4 presumably varies from micelle to micelle. The presence of SiQDs and iron oxide in the MSiQD-Mag was verified by energy-dispersive X-ray (EDX) analysis, as shown in Figure 1F, indicating that silicon and iron oxide were colocalized in the core of the micelle.

The multiple magnetic particles coencapsulated with the SiQDs in the core of the micelle can yield combined properties of both materials in one nanoprobe. Figure 2 shows the result of placing a magnet behind a vial containing the coencapsulated nanoparticles. In the presence of this externally applied magnetic field, the particles are magnetized and drawn through solu-

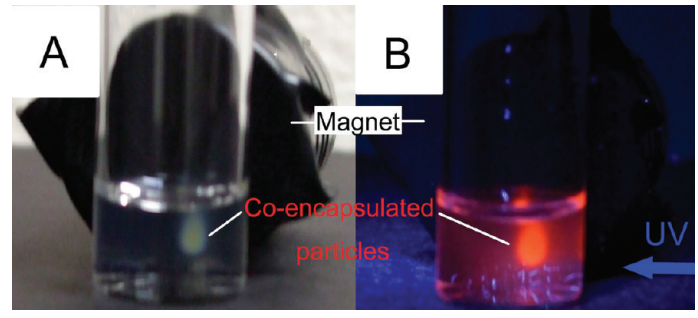

Figure 2. Manipulation of MSiQD-Mag nanoprobes with an external magnetic field. Particles move out of solution and localize on a spot close to the magnet while maintaining their optical properties: (A) under white light illumination; (B) illuminated with a 365 nm UV lamp.

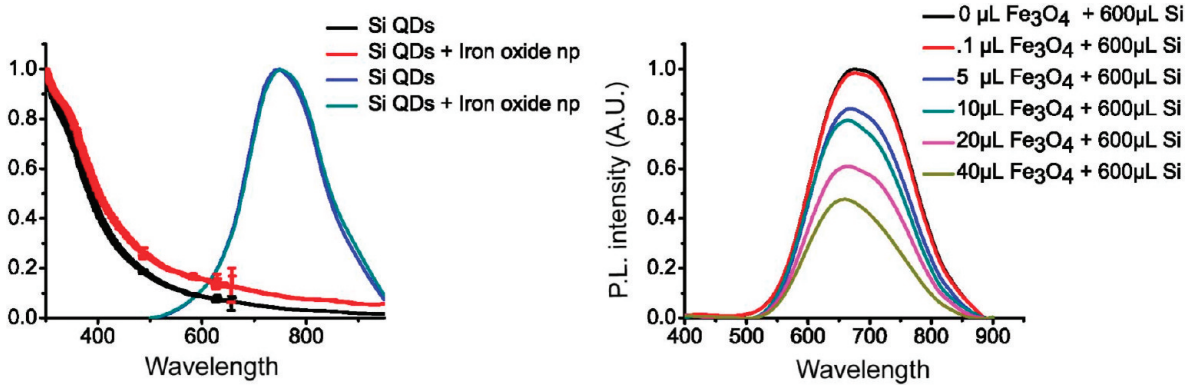

Figure 3. Optical properties of the coencapsulated silicon and iron oxide nanoparticles. (A) Normalized absorption profiles of SiQDs in the absence and presence of magnetic NPs; also shown is the photoluminescence emission spectrum of MSiQDs with and without coencapsulation of iron oxide in the micelle core. (B) Effect of coencapsulated magnetic NPs on the emission spectra of SiQD-containing micelles with increasing amounts of iron oxide.

tion to localize at a point where the field gradient is the strongest. Upon removal of the magnetic field and swirling the vial gently, the particles quickly resuspend in solution. The superparamagnetic property of the hybrid micelle-encapsulated nanoparticles stems from iron oxide NPs, and it is not observed when a magnet is applied to MSiQDs without the iron oxide particles in the core. When excited with UV light (350 nm), the particles emit intense luminescence even under the influence of a magnetic field and after spatial localization of the particles.

Figure 3A shows the absorption and the emission spectra of the micelle-encapsulated silicon quantum dots with and without coencapsulation of the iron oxide nanoparticles. The spectra from the coencapsulated particles are similar to those from the MSiQD. However, with increasing amounts of iron oxide, there is increased absorption above 400 nm. This may be due to increased scattering from larger particles or the added absorbance from iron oxide nanoparticles. Attenuation of fluorescence of the silicon QDs occurs, as expected,[9] as shown in Figure 3B. Details of the fluorescence quenching mechanism require further investigation, beyond the scope of the present article. Because the concentration of the iron oxide nanoparticles increases while that of the silicon quantum dots stays the same, the iron oxide nanoparticles could be displacing silicon quantum dots that otherwise would have been in the micelle. Iron oxide nanocrystals can also potentially quench QD fluorescence through energy transfer. The increased absorbance seen in Figure 3A could also attenuate the excitation light and, thus, the emitted fluorescence.[9]

Temperature is another important parameter for biological experiments (*e.g.*, in cell-incubation studies, polymerase chain reaction (PCR), DNA sensors).[24] Figure 4 depicts the optical properties of the coencapsulated particles as a function of temperature. As the temperature increases, the luminescence decreases, in agreement with previous reports.[24] From 20 to 70 °C, the luminescence of the particles that emit at 700, 650, and 600 nm decreases by ~15, ~25, and ~40%, respectively. Longer wavelength emitting silicon quantum dots have previously been noted to be more stable under aggressive conditions.[25] This is important because they fall into the desirable near-infrared window (700−900 nm) that is optimal for biological imaging. Even though most biological working temperatures are around 37 °C, some applications could require AC magnetic or photothermal heating of the iron oxide nanoparticles. The temperature stability of MSiQD-Mag nanoprobes may be an advantage if used in those cases. The mechanism of the decrease in fluorescence intensity with rising temperature merits further investigation.

Magnetic characterization was performed using a vibrating sample magnetometer (VSM). Field-dependent magnetization plots illustrated that both iron oxide NPs and MSiQD-Mag were superparamagnetic at 305 K (Figure 5). Iron oxide NPs alone showed higher magnetization (emu per gram at saturation) compared to MSiQD-Mag, as expected given the small mass fraction of Fe_3O_4 in the coencapsulated samples. However, when normalized, the magnetization profiles of the samples were nearly identical.

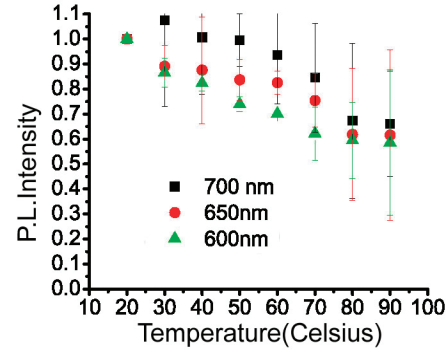

Figure 4. Emission of MSiQD-Mag with increasing temperature. Particles of different sizes and emission wavelengths show similar trends; however, larger particles with longer emission wavelength have greater thermal stability.

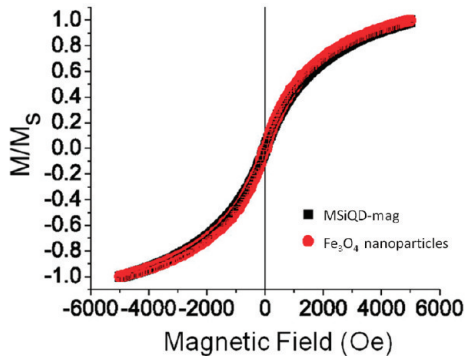

Figure 5. Normalized magnetic moment *vs* magnetic field for Fe_3O_4 alone, and coencapsulated particles.

Stability and Imaging. We previously demonstrated that silicon quantum dots could be used for cellular imaging with nonspecific uptake of amine-terminated micelles or targeted uptake of transferrin-conjugated micelles by cells expressing transferring receptors.[15] To demonstrate magnetic guidance and bioimaging capabilities of the multimodal particles, we chose macrophage cells as the target cell line with nontargeted (methoxy-terminated) micelles. The day prior to the experiment, the cells were seeded in 35 mm cell culture dishes at 70−80% confluence. On the day of the experiment, the cells were incubated for 2 h with methoxy-PEG-terminated MSiQD-Mag. A magnet was put under one sample dish, while the control dish was not exposed to a magnetic field. Figure 6 shows confocal microscopic images of RAW cells incubated with MSiQD-Mag. Figure 6 (top) shows cells incubated without a magnetic field, while for the cells shown in Figure 6 (bottom), the MSiQD-Mag was guided by the magnetic field gradient. Figure 6 (top), from the control dish, shows that without the magnetic field gradient minimal uptake was observed. These results suggest that the manipulation of MSiQD-Mag could locally increase the uptake by cells with the aid of the magnetic force and that uptake could be optically tracked with fluorescence microscopy.

Figure 7 presents spectral imaging results obtained using MSiQD-Mag probes directly injected into the tumor xenograft of a tumor-bearing mouse and monitored over time to detect luminescence stability within the tumor microenvironment. The white light image of Figure 7a shows the tumor locations on the mouse. Figure 7b shows the corresponding luminescence image for MSiQD-Mag and MSiQDs signals at the tumor site compared to autofluorescence of the mouse. Figure 7c shows bright luminescence from MSiQD-Mag and MSiQDs 24 h post-injection. Previously reported times for maintenance of QD luminescence in a tumor site are typically 6−8 h.[26] Thus, if MSiQDs are targeted to the tumor site, they may be stable longer than the typical duration of quantum dots at the tumor location. There is an 8 ± 5 nm red shift for both the MSiQDs and MSiQD-Mag particles from 0 to 24 h, as noted in Figure 7d, and the particles maintain similar emission profiles that are easily distinguishable from the autofluorescence of the mouse. The overall signal intensity after 24 h is 20% higher than the intensity immediately after injection. There are no previous studies on the stability of luminescence of magnetic silicon quantum dot complexes in the tumor microenvironment for comparison. However, this intensity increase may be related to the fact that silicon luminescence intensity typically rises with decreasing pH, and the tumor microenvironment is expected to be acidic. In addition to complementing the stability data in biologically relevant solvents, Figure 7e, these results suggest the MSiQDs and MSiQD-Mag par-

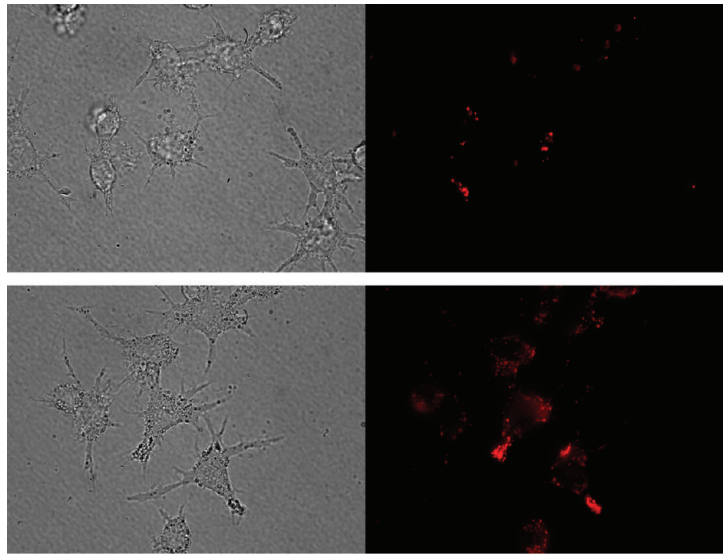

Figure 6. Cellular Imaging. Macrophage RAW cells treated with MSiQD-Mag NP, (top) without and (bottom) with a magnet placed under the culture dish. The exposure time used in the bottom panels was half that used in top panels, but all other imaging conditions were identical.

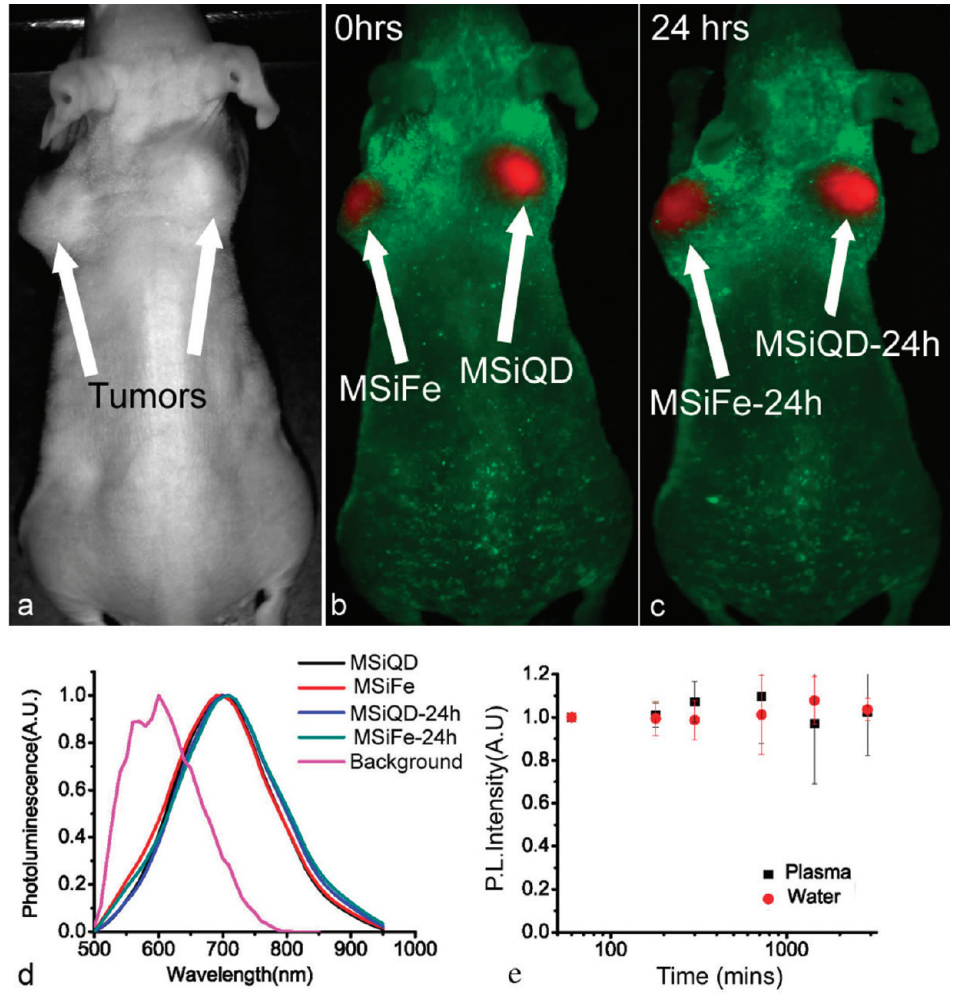

Figure 7. Tests of MSiQD-Mag and MSiQD stability in the prostate cancer tumor microenvironment. (a) White-light image showing tumor locations on the mouse; (b) corresponding pseudocolor luminescence image, with the MSiQD-Mag and MSiQD signals at the tumor site spectrally unmixed from autofluorescence; (c) equivalent luminescence image 24 h post-injection; (d) emission spectra from MSiQD-Mag and MSiQD particles *in vivo*, along with the autofluoresence spectrum; and (e) quantitative measurements of stability of emission from MSiQD-Mag particles in water and plasma. Note that MSiFe is a shorter alternative notation for MSiQD-Mag.

ticles can be relevant for tumor targeting. Figure 7e shows that MSiQD-Mag is stable and does not lose significant luminescence in water or in bovine serum plasma. This also illustrates the potential generality of this approach. Just as iron oxide NPs can replace some SiQDs during the micelle encapsulation, other hydrophobic moieties, including chemotherapeutic drugs, might similarly be coencapsulated. Thus, traceable drug delivery might also be a possibility by coencapsulating SiQDs with a chemotherapeutic drug such as paclitaxel.

Over the past few years, many research groups have developed novel approaches to fabricate nanostructures combining QD photoluminescence with magnetic properties for biological applications. For example, Santra *et al.*[27] have reported the production of CdS:Mn/ZnS core−shell QDs, which possess fluorescence, radioopacity, and paramagnetic properties for *in vivo* bioimaging. They have demonstrated that TAT peptide-labeled QDs can be used as an optical indicator to stain brain blood vessels in small animals. Selvan *et al.*[28] demonstrated the preparation of a bifunctional nanocomposite system consisting of Fe_2O_3 magnetic nanoparticles and CdSe QDs. More specifically, CdSe QDs were grown onto Fe_2O_3 cores, forming either heterodimers or a homogeneous dispersion of QDs around the cores. The resulting QDs displayed both superparamagnetism and tunable optical emission properties. Subsequently, the QD surfaces were further functionalized with biocompatible polymers and targeting molecules for use as probes for labeling live cell membranes. These results have demonstrated that QDs can serve as a key component of versatile multimodal probes, designed for specific biological applications. However, most previous examples have employed cadmium-based QDs, which significantly impedes their broad application due to their potential toxicity issues. Silicon-based QDs appear to be a good alternative to replace cadmium-containing QDs in some applications, due to their inherent biocompatibility. By packaging both silicon QDs and magnetite nanoparticles in a single nanoprobe us-

ing PEGylated phospholipids, it may ultimately be possible to develop magnetically guided traceable drug delivery for cancer therapy that will minimize collateral damage to normal tissues and allow tracking of delivery and efficacy of the therapy.

CONCLUSION

We have produced a magnetofluorescent probe with luminescence and superparamagnetic properties by combining SiQDs and iron oxide NPs. This opens the door to optimizing SiQD-based nanocarriers that might be extended to serve as a multimodal platform incorporating other agents of interest, including plasmonic gold nanostructures, therapeutic drugs, or Si-RNA. This approach shows the tremendous promise of SiQDs as a component of probes for multimodal imaging and therapy.

EXPERIMENTAL METHODS

Photoluminescent Silicon QD Preparation. Silicon nanocrystals were prepared by CO_2 laser pyrolysis of silane in an aerosol reactor based on the method developed by Li *et al.*[29,30] The resulting powder consisted of nonphotoluminescent crystalline Si particles about 5−10 nm in diameter. The etching procedure developed by Hua *et al.*[31] was adopted and modified to reduce the nanocrystal size and break up agglomerated nanocrystals. A 30 mg portion of the Si powder was dispersed in 3 mL of methanol with sonication. An 11 mL aliquot of an acid mixture containing HF (48 wt %) and HNO_3 (69 wt %) (10/1, v/v) was added to the resulting dispersion to initiate etching. As the etching proceeded, the particle size decreased, resulting in visible PL that evolved from infrared to red to yellow to green. Upon approaching the desired emission color, etching was slowed by adding about 20 mL of methanol. The particles were collected on a poly(vinylidene fluoride) (PVDF) membrane filter (nominal pore size 100 nm) and washed with a large amount of 1:3 methanol/water mixture to remove any adsorbed acid mixture. The particles were rinsed with pure methanol and then added to the reagent to be used for the photoinitiated hydrosilylation. This process was performed under a nitrogen atmosphere. Sonication was used to disperse the particles, but a stable colloidal dispersion was not formed, and the reactor contents appeared cloudy in all cases. The mixtures were transferred into a 40 mL Aldrich Schlenk-type reactor containing a magnetic stirrer. A Rayonet photochemical reactor (Southern New England Ultraviolet Co.) equipped with 16 RPR-2537 Å UV tubes was used to initiate the hydrosilylation reaction. The reaction time required varied substantially depending on the compound being attached to the particles and the particle size. After reaction, a clearer dispersion was obtained. It was drawn through a PTFE syringe filter (pore size 0.45 μm).

Fe_3O_4 NP Preparation. Monodispersed (~7 nm) magnetite nanoparticles were synthesized by the method of Sun *et al.*[32] Briefly, the precursors, iron(III) acetylacetonate (2 mmol) and 1,2-hexadecanediol (10 mmol), were mixed with oleic acid (6 mmol) and oleylamine (6 mmol) in 20 mL of phenyl ether. The mixture was put into a three-neck flask under argon gas and was heated to 265 °C (509 °F) for 30 min. After cooling, ethanol was added to the dark brown solution and the magnetite nanoparticles were precipitated by centrifugation (15 000 rpm, 15 min). The precipitate could be redispersed in chloroform or hexane.

Micelle Encapsulation. The encapsulation procedure previously reported by our group was modified slightly for coencapsulation. In a typical experiment, 10 mg of the phospholipid was dispersed in 1.0 mL of chloroform in a 100 mL round-bottom flask. A 600 μL portion of silicon quantum dot dispersion (containing ~8 mg of silicon) was mixed with varying amounts of iron oxide nanoparticle dispersion (0.1 to 40 μL of a dispersion containing ~20 mg/mL Fe_3O_4). Unless otherwise specified, 5 μL was used in all subsequent experiments, corresponding to a Si to Fe_3O_4 ratio of about 80:1 by mass. Each mixture was gently stirred for 5 to 40 min. A Labconco rotary evaporator with a water bath of 37 °C was used to evaporate the solvents. The lipidic film, deposited on the reaction vial, was hydrated with 3−5 mL of HPLC water and subjected to ultrasonication for 10 min using a bath sonicator. The resulting dispersion was filtered through a 0.2 μm membrane filter and kept at 4 °C for further use.

Photoluminescence and PLE Spectra. Photoluminescence (PL) spectra were recorded using a Perkin-Elmer luminescence spectrometer (model LS50) with a 390 nm emission cutoff filter. The excitation wavelength was set at 350 nm and the emission scanned from 400 to 800 nm. Solution samples of grafted silicon particles were filtered through a syringe filter (PTFE, pore size 450 nm), diluted to a concentration of about 0.01 g/L, and then loaded into a quartz cuvette for measurements.

Temperature Study. SiQDs of different sizes, coencapsulated with 5 μL of Fe_3O_4 dispersion to yield a Si to Fe_3O_4 ratio of about 80:1 (by mass) were dispersed in water and heated. Samples of the QD solution were extracted at temperatures ranging from ambient to 100 °C, and the photoluminescence was immediately measured as described above.

Macrophage Cell Culture. RAW264.7 cells lines were obtained from the American Type Culture Collection (ATCC: No. TIB-71). They were cultured in Dulbecco's modified Eagle's medium (DMEM), supplemented with 10% fetal bovine serum, penicillin (100 U/mL), and streptomycin (100 μg/mL) at 37 °C in a humidified atmosphere of 95% air and 5% CO_2, and the medium was changed every other day. Cells were plated onto 35 mm tissue culture dishes at 5×10^5 cells/dish or onto 60 mm dishes at 1.5×10^6 cells/dish or onto 96-well plates at 5.0×10^4 cells/well on the day prior to experiments.

Prostate Cancer Cell Lines. PC-3 cells were obtained from American Type Tissue Collection (ATCC). Cells were maintained in DMEM high glucose medium (Sigma-Aldrich, St. Louis, MO) containing 10% FBS (Sigma-Aldrich), 1 mM L-glutamine (Sigma-Aldrich), 100 μg/mL kanamycin (Sigma-Aldrich), and 0.5 μg/mL amphotericin B (Sigma-Aldrich) in a 75 cm^2 nunclon delta treated flask (Nun A/S, Rockskilde, Denmark).

For xenograph preparation, an 85−90% confluent cell flask was rinsed three times with sterile DPBS (Sigma-Aldrich). Five milliliters of a trypsin-EDTA (Sigma-Aldrich) solution was added to the flask and incubated at 37 °C and 5% CO_2 until cells released. Once the cells were released, 5 mL of the medium was added to the trypsin, and the entire flask contents were removed and placed in a sterile 50 mL centrifuge tube (Becton Dickenson Labware, Franklin Lakes, NJ). The cells were spun down at 2000 rpm for 5 min, and the supernatant was removed. The cell pellet was resuspended in 5 mL of fresh media, and a cell count using trypan blue (Sigma-Aldrich) was performed. On the basis of the concentration of cells needed per injection, a 1:1 mixture of cell suspension and Matrigel (BD Biosciences, Bedford, MA) was made.

Xenograph Tumor Model. Five to six week old female athymic nude mice (Hsd:Athymic Nude-*Foxn1^{nu}*) were obtained from Harlan Laboratories, Inc., and allowed an acclimation period of 1 week. The nude mice were housed in sterile M.I.C.E caging (Animal Care Systems, Centennial Co.) that contained sterile bedding, food, and water. Animal care was set up in accordance with the guidelines of the Institutional Animal Care and Use Committee (IACUC) established at the University of Buffalo.

Human prostate tumor models were created in the athymic mice by injecting PC-3 cells at concentrations of $2-3 \times 10^6$ cells in a 100 μL suspension of Matrigel (BD Biosciences) and medium mixture (1:1) maintained at 4 °C. This mixture was then injected subcutaneously in one scapular region of the mice using a 1 mL Monoject tuberculin syringe with a 25 g × 5/8 in. detachable needle (Tyco Healthcare Group, LP, Mansfield, MA). Tumor growth was monitored every 24−48 h until tumor size of approximately 5 mm^2 was obtained 10−14 days post-transplantation of cells.

Once tumors reached the appropriate size, the mice were injected with various concentrations of micelle-encapsulated silicon quantum dots or coencapsulated silicon quantum dots and iron oxide nanoparticles by direct tumor injection at a volume of 150−200 μL per injection. After injection, mice were anesthe-

tized with 3% aerrane/isoflurane/1 L O_2. Anesthesia maintenance concentrations were 2−3% isoflurane/1 L O_2. Once the proper plane of anesthesia was reached, the mice were imaged using the Maestro *in vivo* optical imaging system (CRI, Inc., Woburn, MA) at specific time points to monitor progress of the micelle-encapsulated quantum dots.

Acknowledgment. This study was supported by grants from the NSF IGERT, NCI R01CA11937, the John R. Oishei Foundation, the Chemistry and Life Sciences Division of the Air force Office of Scientific Research, the University at Buffalo Gerald Sterbutzel Fund, and the University at Buffalo Interdisciplinary Research and Creative Activities fund.

Supporting Information Available: Additional figures. This material is available free of charge *via* the Internet at http://pubs.acs.org.

REFERENCES AND NOTES

1. Prasad, P. N. *Biophotonics*; Wiley-Interscience: Hoboken, NJ, 2003.
2. Prasad, P. N. *Nanophotonics*; Wiley-Interscience: Hoboken, NJ, 2004.
3. Shi, C.; Zhu, Y.; Cerwinka, W. H.; Zhau, H. E.; Marshall, F. F.; Simons, J. W.; Nie, S.; Chung, L. W. K. Quantum Dots: Emerging Applications in Urologic Oncology. *Urol. Oncol.: Semin. Orig. Invest.* **2008**, *26*, 86–92.
4. Derfus, A. M.; Chan, W. C. W.; Bhatia, S. N. Probing the Cytotoxicity of Semiconductor Quantum Dots. *Nano Lett.* **2004**, *4*, 11–18.
5. Kirchner, C.; Liedl, T.; Kudera, S.; Pellegrino, T.; MunozJavier, A.; Gaub, H. E.; Stolzle, S.; Fertig, N.; Parak, W. J. Cytotoxicity of Colloidal CdSe and CdSe/ZnS Nanoparticles. *Nano Lett.* **2005**, *5*, 331–338.
6. Ron, H. A Toxicologic Review of Quantum Dots: Toxicity Depends on Physicochemical and Environmental Factors. *Environ. Health Perspect.* **2006**, *114*, 165–172.
7. Park, J.-H.; von, G.; Ruoslahti, M. E.; Bhatia, S. N.; Sailor, M. J. Micellar Hybrid Nanoparticles for Simultaneous Magnetofluorescent Imaging and Drug Delivery. *Angew. Chem., Int. Ed.* **2008**, *47*, 7284–7288.
8. Insin, N.; Tracy, J. B.; Lee, H.; Zimmer, J. P.; Westervelt, R. M.; Bawendi, M. G. Incorporation of Iron Oxide Nanoparticles and Quantum Dots into Silica Microspheres. *ACS Nano* **2008**, *2*, 197–202.
9. Sathe, T. R.; Agrawal, A.; Nie, S. Mesoporous Silica Beads Embedded with Semiconductor Quantum Dots and Iron Oxide Nanocrystals: Dual-Function Microcarriers for Optical Encoding and Magnetic Separation. *Anal. Chem.* **2006**, *78*, 5627–5632.
10. Wang, D.; He, J.; Rosenzweig, N.; Rosenzweig, Z. Superparamagnetic Fe_2O_3 Beads-CdSe/ZnS Quantum Dots Core−Shell Nanocomposite Particles for Cell Separation. *Nano Lett.* **2004**, *4*, 409–413.
11. Lee, J.; Hasan, W.; Lee, M. H.; Odom, T. W. Optical Properties and Magnetic Manipulation of Bimaterial Nanopyramids. *Adv. Mater.* **2007**, *19*, 4387–4391.
12. Law, W.-C.; Yong, K.-T.; Roy, I.; Xu, G.; Ding, H.; Bergey, E. J.; Zeng, H.; Prasad, P. N. Optically and Magnetically Doped Organically Modified Silica Nanoparticles as Efficient Magnetically Guided Biomarkers for Two-Photon Imaging of Live Cancer Cells. *J. Phys. Chem. C* **2008**, *112*, 7972–7977.
13. Xu, H.; Wu, H.; Huang, F.; Song, S.; Li, W.; Cao, Y.; Fan, C. Magnetically Assisted DNA Assays: High Selectivity Using Conjugated Polymers for Amplified Fluorescent Transduction. *Nucleic Acids Res.* **2005**, *33*, e83-.
14. Hahn, P. F.; Stark, D. D.; Lewis, J. M.; Saini, S.; Elizondo, G.; Weissleder, R.; Fretz, C. J.; Ferrucci, J. T. First Clinical Trial of a New Superparamagnetic Iron Oxide for Use as an Oral Gastrointestinal Contrast Agent in MR Imaging. *Radiology* **1990**, *175*, 695–700.
15. Erogbogbo, F.; Yong, K.-T.; Roy, I.; Xu, G.; Prasad, P. N.; Swihart, M. T. Biocompatible Luminescent Silicon Quantum Dots for Imaging of Cancer Cells. *ACS Nano* **2008**, *2*, 873–878.
16. Fujioka, K.; Hiruoka, M.; Sato, K.; Manabe, N.; Miyasaka, R.; Hanada, S.; Hoshino, A.; Tilley, R. D.; Manome, Y.; Hirakuri, K.; Yamamoto, K. Luminescent Passive-Oxidized Silicon Quantum Dots as Biological Staining Labels and Their Cytotoxicity Effects at High Concentration. *Nanotechnology* **2008**, *19*, 415102.
17. Park, J.-H.; Gu, L.; von Maltzahn, G.; Ruoslahti, E.; Bhatia, S. N.; Sailor, M. J. Biodegradable Luminescent Porous Silicon Nanoparticles for *In Vivo* Applications. *Nat. Mater.* **2009**, *8*, 331–336.
18. Choi, J.; Wang, N. S.; Reipa, V. Conjugation of the Photoluminescent Silicon Nanoparticles to Streptavidin. *Bioconjugate Chem.* **2008**, *19*, 680–685.
19. Mangolini, L.; Jurbergs, D.; Rogojina, E.; Kortshagen, U. High Efficiency Photoluminescence from Silicon Nanocrystals Prepared by Plasma Synthesis and Organic Surface Passivation. *Phys. Status Solidi C* **2006**, *3*, 3975–3978.
20. He, G. S.; Zheng, Q.; Yong, K.-T.; Erogbogbo, F.; Swihart, M. T.; Prasad, P. N. Two- and Three-Photon Absorption and Frequency Upconverted Emission of Silicon Quantum Dots. *Nano Lett.* **2008**, *8*, 2688–2692.
21. Erogbogbo, F.; Yong, K.-T.; Roy, I.; Hu, R.; Law, W.-C.; Zhao, W.; Ding, H.; Wu, F.; Kumar, R.; Swihart, M. T.; Prasad, P. N. *In Vivo* Targeted Cancer Imaging, Sentinel Lymph Node Mapping and Multi-channel Imaging with Biocompatible Silicon Nanocrystals. *ACS Nano* Submitted for publication.
22. Zhang, X.; Brynda, M.; Britt, R. D.; Carroll, E. C.; Larsen, D. S.; Louie, A. Y.; Kauzlarich, S. M. Synthesis and Characterization of Manganese-Doped Silicon Nanoparticles: Bifunctional Paramagnetic-Optical Nanomaterial. *J. Am. Chem. Soc.* **2007**, *129*, 10668–10669.
23. Dubertret, B.; Skourides, P.; Norris, D. J.; Noireaux, V.; Brivanlou, A. H.; Libchaber, A. *In Vivo* Imaging of Quantum Dots Encapsulated in Phospholipid Micelles. *Science* **2002**, *298*, 1759–1762.
24. Jiang, W.; Mardyani, S.; Fischer, H.; Chan, W. C. W. Design and Characterization of Lysine Cross-Linked Mercapto-Acid Biocompatible Quantum Dots. *Chem. Mater.* **2006**, *18*, 872–878.
25. Hua, F. J.; Erogbogbo, F.; Swihart, M. T.; Ruckenstein, E. Organically Capped Silicon Nanoparticles with Blue Photoluminescence Prepared by Hydrosilylation Followed by Oxidation. *Langmuir* **2006**, *22*, 4363–4370.
26. Cai, W.; Shin, D. W.; Chen, K.; Gheysens, O.; Cao, Q.; Wang, S. X.; Gambhir, S. S.; Chen, X. Peptide-Labeled Near-Infrared Quantum Dots for Imaging Tumor Vasculature in Living Subjects. *Nano Lett.* **2006**, *6*, 669–676.
27. Santra, S.; Yang, H.; Holloway, P. H.; Stanley, J. T.; Mericle, R. A. Synthesis of Water-Dispersible Fluorescent, Radio-Opaque, and Paramagnetic CdS:Mn/ZnS Quantum Dots: A Multifunctional Probe for Bioimaging. *J. Am. Chem. Soc.* **2005**, *127*, 1656–1657.
28. Ang, C. Y.; Giam, L.; Chan, Z. M.; Lin, A. W. H.; Gu, H.; Devlin, E.; Papaefthymiou, G. C.; Selvan, S. T.; Ying, J. Y. Facile Synthesis of Fe_2O_3 Nanocrystals without Fe(CO)5 Precursor and One-Pot Synthesis of Highly Fluorescent Fe_2O_3-CdSe Nanocomposites. *Adv. Mater.* **2009**, *21*, 869–873.
29. Li, X. G.; He, Y. Q.; Swihart, M. T. Surface Functionalization of Silicon Nanoparticles Produced by Laser-Driven Pyrolysis of Silane Followed by HF-HNO_3 Etching. *Langmuir* **2004**, *20*, 4720–4727.
30. Li, X. G.; He, Y. Q.; Talukdar, S. S.; Swihart, M. T. Process for Preparing Macroscopic Quantities of Brightly Photoluminescent Silicon Nanoparticles with Emission Spanning the Visible Spectrum. *Langmuir* **2003**, *19*, 8490–8496.
31. Hua, F. J.; Swihart, M. T.; Ruckenstein, E. Efficient Surface Grafting of Luminescent Silicon Quantum Dots by Photoinitiated Hydrosilylation. *Langmuir* **2005**, *21*, 6054–6062.
32. Sun, S.; Zeng, H. Size-Controlled Synthesis of Magnetite Nanoparticles. *J. Am. Chem. Soc.* **2002**, *124*, 8204–8205.